AD-A173 966 A COMPARISON OF RADIATION TRANSPORT METHODS IN AXISYMMETRIC GEOMETRIES(U) NAVAL RESEARCH LAB WASHINGTON DC J L GIULIANI 06 OCT 86 NRL-MR-5871 1/1

UNCLASSIFIED F/G 20/13 NL

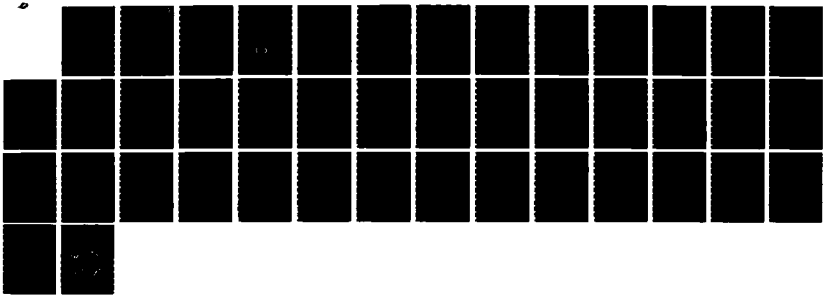

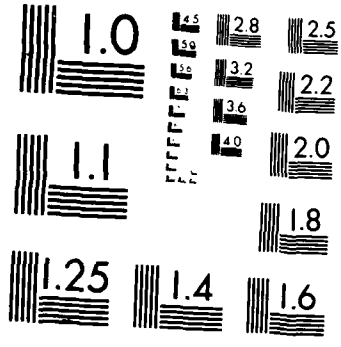

Naval Research Laboratory

Washington, DC 20375-5000 NRL Memorandum Report 5871 October 6, 1986

A Comparison of Radiation Transport Methods in Axisymmetric Geometries

JOHN L. GIULIANI, JR.

Geophysical and Plasma Dynamics Branch
Plasma Physics Division

This work was supported by the Defense Nuclear Agency under Subtask code and title RL RA/Advanced Simulation Concepts, work unit code and title, 00049/X-ray Source Development Theory.

Approved for public release; distribution unlimited

SECURITY CLASSIFICATION OF THIS PAGE

REPORT DOCUMENTATION PAGE

A173966

1a REPORT SECURITY CLASSIFICATION UNCLASSIFIED	1b RESTRICTIVE MARKINGS
2a SECURITY CLASSIFICATION AUTHORITY	3 DISTRIBUTION/AVAILABILITY OF REPORT Approved for public release; distribution unlimited.
2b DECLASSIFICATION/DOWNGRADING SCHEDULE	
4 PERFORMING ORGANIZATION REPORT NUMBER(S) NRL Memorandum Report 5871	5 MONITORING ORGANIZATION REPORT NUMBER(S)
6a NAME OF PERFORMING ORGANIZATION Naval Research Laboratory	6b OFFICE SYMBOL (If applicable) 4720
6c ADDRESS (City, State, and ZIP Code) Washington, DC 20375-5000	7a NAME OF MONITORING ORGANIZATION 7b ADDRESS (City, State, and ZIP Code)
8a NAME OF FUNDING/SPONSORING ORGANIZATION Defense Nuclear Agency	8b OFFICE SYMBOL (If applicable) RAEV
8c ADDRESS (City, State, and ZIP Code) Alexandria, Virginia 22310	9 PROCUREMENT INSTRUMENT IDENTIFICATION NUMBER

10 SOURCE OF FUNDING NUMBERS

PROGRAM ELEMENT NO	PROJECT NO	TASK NO	WORK UNIT ACCESSION NO
62715H		RL RA	DN880-191

11 TITLE (Include Security Classification)
A Comparison of Radiation Transport Methods in Axisymmetric Geometries

12 PERSONAL AUTHOR(S)
Giuliani, Jr. John L.

13a TYPE OF REPORT	13b TIME COVERED	14 DATE OF REPORT (Year, Month, Day)	15 PAGE COUNT
Interim	FROM _____ TO _____	1986 October 6	42

16 SUPPLEMENTARY NOTATION
This work was supported by the Defense Nuclear Agency under Subtask code and title RL RA/Advanced Simulation Concepts, work unit code and title 00049/X-ray Source DevelopmentTheory.

17 COSATI CODES			18 SUBJECT TERMS (Continue on reverse if necessary and identify by block number)
FIELD	GROUP	SUB-GROUP	Radiation-hydrodynamics Radiation transport Numerical methods

19 ABSTRACT (Continue on reverse if necessary and identify by block number)

The radiative transfer equation with a fixed source and fixed absorption is studied in axisymmetric geometries. A comparison of solutions for several model problems is presented using two different numerical schemes. The first scheme uses the radiation diffusion approximation with flux-limiting; the second, a multi-directional ray trace. The underlying spatial grid over which the solutions are calculated is a distorted set of quadrilaterals for application to two dimensional, Lagrangian, radiation-hydrodynamic codes.

The results of the numerical solutions indicate that both schemes are accurate in radiating, optically thick regions. In source-free, purely absorbing regions, the accuracy decreases, but much more so for the diffusion approach than the ray tracing one. The major advantages of the latter approach over the former are; (i) the accuracy can be easily improved by increasing the number of rays for example, and (ii) computation time can be shorter for multi-frequency calculations with more than about 10 frequencies.

20 DISTRIBUTION/AVAILABILITY OF ABSTRACT	21 ABSTRACT SECURITY CLASSIFICATION
☒ UNCLASSIFIED/UNLIMITED ☐ SAME AS RPT ☐ DTIC USERS	UNCLASSIFIED

22a NAME OF RESPONSIBLE INDIVIDUAL	22b TELEPHONE (Include Area Code)	22c OFFICE SYMBOL
Dr. Jack Davis,	202-767-3278	4720

DD FORM 1473, 84 MAR 83 APR edition may be used until exhausted
All other editions are obsolete

SECURITY CLASSIFICATION OF THIS PAGE

U.S. Government Printing Office 1985-607-047

CONTENTS

A COMPARISON OF RADIATION TRANSPORT METHODS IN AXISYMMETRIC GEOMETRIES

I. INTRODUCTION

Radiation from a plasma and its subsequent transport through a surrounding medium is a fundamental physical process in several experiments presently ongoing at the Naval Research Laboratory. In the laser-target interaction of the PHAROS III experiment, radiation plays an important role in heating the backside of the target leading to the rearward plasma blowoff.[1] Radiation from atomic lines is one of the few diagnostics available to study the dynamics of the hot, shocked cavity of ambient gas formed by the frontside blowoff.[2] One aim of the Z-pinch of the GAMBLE II facility is to create a highly energetic burst of x-rays at maximum compression on axis,[3] and another one is possibly to develop an x-ray laser.

Although both of these experiments have been modeled with one dimensional radiation-hydrodynamic numerical codes (Refs. above), there are certain aspects which require at least a two dimensional treatment. For instance, the plasma blowoff from a laser target is asymmetric about the plane of the target, though nearly symmetric about the laser axis. And a sausage or Rayleigh-Taylor instability about the compression axis can disrupt a uniform Z-pinch which is required for maximum efficiency.

Furthermore, both experiments involve large changes in length scales from the initial configuration to the final one. In the laser-target interaction, the disturbed plasma expands from the size of the target, a few microns, to nearly a centimeter at blast wave formation. In the Z-pinch, the annular gas puff starts at about a centimeter in radius and compresses to less than a tenth of this radius. Hence a Lagrangian or an adaptive spatial mesh is needed to follow the plasma with proper resolution.

This report addresses the problem of how to solve the radiation transfer equation in an axisymmetric geometry over an arbitrary quadrilateral mesh in

Manuscript approved June 30, 1986

the R-Z computational plane. Two numerical schemes are considered. The first scheme is a generalization of the Eddington diffusion approximation for radiation transfer wherein the radiation flux is proportional to the gradient of the radiation energy density. It uses a simple flux-limiter to constrain the radiation flux to physical values in regions of steep gradients. The resulting equation for the radiation energy density is a diffusive one and is solved by a matrix inversion technique over the spatial mesh. The second scheme is more direct. It solves the radiative transfer equation along a set of rays in three-dimensional space extending from each cell center in the distorted two-dimensional mesh. The resulting intensities are then averaged to get the local radiation energy density.

The present ray trace scheme is a generalization of the one proposed by Colombant and Winsor[4,5] and used in a laser target model[6]. Their earlier approach performed a crude average of intensities for rays outside of the computational plane and was restricted to square meshes in that plane.

The solutions from the diffusion and ray trace schemes are compared against a closed form solution of the radiative transfer equation for an emitting cylindrical core in Section II. The schemes are also compared against each other for problems of more complex configurations. Each scheme has its advantages and disadvantages as will be pointed out below in the Conclusions, Section III.

Let us begin by discussing two different formal solutions of the radiative transfer equation. Let $I(\mathbf{r},\Omega,\nu,t)$ be the specific intensity at position $\mathbf{r}$, in the unit vector direction Ω, at frequency ν and time t, with units of ergs/cm^2·sec·Hz·steradian. Let $\sigma_a(\mathbf{r},\nu,t)$ be the pure absorption coefficient with units of cm^{-1}, and likewise $\sigma_s(\mathbf{r},\nu,t)$ the pure scattering coefficient. Finally let $\varepsilon(\mathbf{r},\nu,t)$ be the isotropic emission coefficient with units of ergs/cm^3·sec·Hz. Then for non-relativistic flows, the transfer equation is[7]

$$\frac{1}{c}\frac{\partial I(\mathbf{r},\Omega,\nu,t)}{\partial t} + \Omega\cdot\nabla\, I(\mathbf{r},\Omega,\nu,t) + [\sigma_a(\mathbf{r},\nu,t)+\sigma_s(\mathbf{r},\nu,t)]I(\mathbf{r},\Omega,\nu,t)$$

$$= \frac{\varepsilon(\mathbf{r},\nu,t)}{4\pi} + c\sigma_s(\mathbf{r},\nu,t)\,\frac{E(\mathbf{r},\nu,t)}{4\pi}\,, \qquad (1)$$

where $\Omega\cdot\nabla$ is the directional derivative along Ω, and

$$E(\mathbf{r},\nu,t) = \frac{1}{c}\int d\Omega\, I(\mathbf{r},\Omega,\nu,t) \qquad (2)$$

is the radiation energy density per unit frequency.

To obtain an integral formulation of the transfer equation applicable to any coordinate system, consider a steady state situation without scattering. Then rewrite eqn. (1) through a transformation of variables as

$$-\frac{d}{ds}\, I(\mathbf{r}-s\Omega,\Omega,\nu) + \sigma_a(\mathbf{r},\nu)I(\mathbf{r}-s\Omega,\Omega,\nu) = \frac{\varepsilon(\mathbf{r}-s\Omega,\nu)}{4\pi}\,,$$

where s (≥ 0) is a distance backward along the direction Ω. Define the optical depth as

$$\tau(\mathbf{r},\mathbf{r}-s\Omega,\nu) = \int_0^s ds'\ \sigma_a(\mathbf{r}-s'\Omega,\nu)\,, \qquad (3)$$

and use the integrating factor $e^{-\tau}$ to obtain the formal solution

$$I(\mathbf{r},\Omega,\nu) = I(\mathbf{r}-s_b\Omega,\nu)\, e^{-\tau(\mathbf{r},\mathbf{r}-s_b\Omega,\nu)}$$

$$+ \int_0^{s_b} ds'\ \frac{\varepsilon(\mathbf{r}-s'\Omega,\nu)}{4\pi}\ e^{-\tau(\mathbf{r},\mathbf{r}-s'\Omega,\nu)}\,, \qquad (4)$$

where s_b is the distance from the point of observation $\mathbf{r}$ to the outer boundary surface along the direction $-\Omega$. The radiation energy density at $\mathbf{r}$ is given by eqn.(2). The essence of the ray tracing scheme is to evaluate eqn.(4) over a set of rays $\{\Omega\}$ for each observation point $\mathbf{r}$.

An alternative approach which includes the time dependence and scattering is to take angular moments of the transfer equation (1). In cylindrical coordinates, $d\Omega = \sin\theta \cdot d\theta \cdot d\phi$,

$$\Omega = \cos\theta\, \mathbf{e}_z + \sin\theta\cdot\cos\phi\, \mathbf{e}_r + \sin\theta\cdot\sin\phi\, \mathbf{e}_\phi \,, \tag{5}$$

and the transfer equation becomes[8]

$$\frac{1}{c}\frac{\partial I}{\partial t} + \frac{\partial I}{\partial r}\sin\theta\cdot\cos\phi + \frac{\partial I}{\partial z}\cos\theta - \frac{1}{r}\frac{\partial I}{\partial \phi}\sin\theta\cdot\sin\phi + (\sigma_a+\sigma_s)I = \frac{\varepsilon}{4\pi} + c\sigma_s\frac{E}{4\pi} \,. \tag{6}$$

In Cartesian geometries Feautrier variables are often employed to transform the transfer equation into a simpler diffusion equation.[9,10] But in an axisymmetric geometry the presence of the angular derivative in eqn.(6) negates this transformation. Taking the zeroth angular moment of eqn.(6) gives

$$\frac{\partial E}{\partial t} + \nabla\cdot\mathbf{F} + c\sigma_a E = \varepsilon \,, \tag{7}$$

where the radiative flux is defined by

$$\mathbf{F}(r,\nu,t) = \int d\Omega\, I(r,\Omega,\nu,t)\Omega \,. \tag{8}$$

It is well known that the moment method suffers from the standard problem of non-closure, for note that the next angular moment,

$$\frac{1}{c}\frac{\partial \mathbf{F}}{\partial t} + c\nabla\cdot\mathbf{P} + (\sigma_a+\sigma_s)\mathbf{F} = 0 \ , \tag{9}$$

introduces the radiation pressure tensor

$$\mathbf{P}(r,\nu,t) = \frac{1}{c}\int d\Omega\ I(r,\Omega,\nu,t)\ \Omega\,\Omega \ . \tag{10}$$

The essence of the diffusion scheme is to cut off the moment development by relating $\mathbf{P} = f\mathbf{E}$, where f is the so called tensor Eddington factor. Neglecting the time derivative in eqn.(9) shows that this relation leads to

$$\mathbf{F} = -\frac{c}{\sigma_a+\sigma_s}\nabla\cdot f\mathbf{E} \ . \tag{11}$$

II. COMPARISON OF NUMMERICAL SOLUTIONS

A. Simple Model Test Problem and Closed Form Solution.

In order to compare the diffusion scheme for solving the radiative transfer equation with the ray tracing scheme we consider an axisymmetric test problem. This first problem should be simple enough that an accurate closed form solution can be obtained, yet it should have the character of a two dimensional structure. Let the computational plane within which the distorted mesh lies extend upward 1 cm in the z-direction, i.e., the symmetry axis, and outward 1 cm in the radial direction. Rotate this square around the symmetry axis to obtain the computational volume depicted in Fig.1. A spatially and temporally constant emissivity of $\varepsilon = 100$ ergs/cm^3·sec·Hz is assumed within a cylindrical volume of height 1 cm and radial extent 0.2 cm. The absorption coefficient within this region is $\sigma_a = 10.0$ cm^{-1}. We neglect scattering processes. Outside of this region there is no source ($\varepsilon = 0$) and the absorption coefficient is 0.1 cm^{-1}. Thus the center of the emitting region is optically thick, while the source free region is purely absorbing and optically thin. Near the source region the problem is nearly planar, but farther out in radius, and near the edges of the computational volume, the finite extent of the source in the z-direction has its effects. We seek the steady state solution to this problem over the distorted mesh shown in Fig.2.

Due to the simple geometry and spatial dependence of the emissivity and absoption coefficients, the specific intensity at an arbitrary point $\mathbf{r}$ in the computational plane can be computed exactly from eqn.(4) along a direction Ω. The vector Ω is defined by the angles θ and ϕ of Fig.1, and from trigonometric relations the optical depth and line integral of eqn.(4)

are evaluated. Then to obtain the radiation energy density at r, the solid angle subtended by the source region at position r is discretized into a large number of θ and ϕ angles. The same procedure is done for the radiative flux of eqn.(8). Finally, we solve for the angular integrated radiation quantities at the center of each cell in Fig.2. The results for the radiation energy density (ERAD) and the normalized z-component of the radiation flux (FZ/c·ERAD) are displayed in the contour plots of Figs.3a and 3b, respectively. The quantity in the parentheses at the top of Fig.3a is the total radiation energy in the whole computational volume.

B. Diffusive Solution.

The essence of any radiation diffusion scheme is a good estimate of the Eddington factor f of eqn.(11). One way to estimate f is to use the results from a simple ray tracing solution, but this defeats the basic purpose of a diffusion approach in an axisymmetric geometry. Several derivations have been proposed for relating F directly to ∇E with a coefficient R that limits $|F|/c \cdot E$ below the streaming limit of unity.[11,12,13,14,15] All of these derivations take the specific intensity to be isotropic about the direction of the radiative flux, and neglect the spatial and temporal dependence of the Eddington factor f. With these assumptions an expression for R can be derived. It is easy to see, however, that in axisymmetric problems the radiation need not be isotropic about the flux direction. Furthermore, as noted by the above cited authors, in source free or scattering free regions these theories predict that the radiative flux immediately attains the streaming limit, i.e., they break down in a purely absorbing medium. The experiments mentioned in the Introduction are characterized by a small

scattering coefficient and a significant region of minimal emission but strong absorption. Any attempt to remedy these flux-limiting theories would be ad hoc, so we use the simplest flux limiting scheme, which itself is ad hoc, namely,

$$\mathbf{F} = - \frac{c}{3(\sigma_a+\sigma_s)+2\frac{|\nabla E|}{E}} \nabla E \ . \tag{12}$$

This formula was used in early versions of LASNEX.[16] In the limit of small gradients, eqn.(12) reduces to the classical Eddington approximation. In regions of steep gradients one finds $|\mathbf{F}| = cE/2$, the proper result for the radiation flux away from a planar source. Thus the flux-limiter of eqn.(12) should be correct near the surface of a cylindrical source. Using eqn.(12) in eqn.(7) gives a diffusion equation for the radiation energy density;

$$\frac{\partial E}{\partial t} - \nabla\cdot\left(\frac{c}{3(\sigma_a+\sigma_s)+2|\nabla E|/E} \right)\nabla E + c\sigma_a E = \varepsilon \ . \tag{13}$$

This equation is differenced over the distorted mesh of Fig. 2 in a nine point stencil, i.e., the difference equation connects nine mesh cells. Nine cells are coupled together instead of the usual five for a two dimensional partial differential equation due to the non-rectangular mesh. The differencing scheme is similar to that discussed by Kershaw[17] and Pert[18]. During a time step the diffusion coefficient in eqn.(13) is held constant and the resulting set of linear algebraic equations for E is solved by an incomplete Crout decomposition and a conjugate gradient iteration. This matrix solver is similar to one described by Hain[19], but with improvements to speed convergence and generalized to allow for a nine point stencil.

The numerical solutions for the radiation energy density (ERAD)and normalized radiation flux in the z-direction (FZ/c*ERAD) are shown in Figs.4a and 4b respectively. The radiation flux is calculated according to the description for the flux-limiter, eqn.(12), after the solution for E has been found. The presented results represent twenty calls to the diffusion solver with a time step of 10^{-10} seconds per call. The steady state solution is assessed by noting minimal changes from the solution with fewer calls. Typically, it initially takes about 12 iterations within the matrix solver per call to reach an error of 10^{-4} in the L_2 norm. The number of iterations drops to several once the steady state is approached. The boundary conditions are reflective along the symmetry axis and Dirichlet with E = 0 outside the remaining boundaries.

C. Ray Tracing Solutions.

The essence of the ray tracing approach is the approximate solution of eqn.(4) over a set of rays extending from each observation point. For any mesh we take the observation points to be the center of the cells. In order to have a general approach applicable to an arbitrary distribution of sources and opacities there are two major differences from the closed form solution used in section II.A.

First, the optical depth and line integral in eqn.(4) are not calculated exactly as for the closed form solution. Instead each ray from an observation point r is broken into a finite number of equal length segments Δs over which the emission and absorption coefficients will be taken to be constant. If the set $\{s_i\}$, $i = 1$ NSRAY demarks the endpoints of the segments, with $s_i > s_{i+1}$, the solution of the transfer equation over a single segment along the direction Ω can be written as

$$I(r,s_{i+1},\Omega,\nu) = I(r,s_i,\Omega,\nu)\, e^{-\sigma_{a,i+1/2}\Delta s} + \frac{\varepsilon_{i+1/2}}{4\pi\sigma_{a,i+1/2}}\left(1 - e^{-\sigma_{a,i+1/2}\Delta s}\right) . \qquad (14)$$

Integration along the ray from the boundary of the computational volume ($s_1 = s_b$) to the observation point at r is accomplished by repeated application of eqn.(14) till $I(r,s_{NSRAY},\Omega,\nu)$ is reached.

Second, for the closed form solution only those rays going through the source region were considered. In the general ray tracing approach, a set of direction angles $\{\Omega_j\}$, j = 1, NRAY, is chosen to cover half the unit sphere about an observation point, and this set is the same for each observation point. Only half the unit sphere need be covered due to the symmetry about the computational plane. In reference to Fig. 1, there are NCOSTH equally spaced values from 1 to -1 for the cosine of the polar angle θ, and NPHI equally spaced angles from 0 to π for the azimuthal angle ϕ. Thus the number of rays along which eqn.(14) is solved is NSRAY = (NCOSTH-2)*NPHI + 2. When account is taken of the symmetry, there are effectively (NCOSTH-2)*(2*NPHI-2) + 2 rays. The weighting assigned to each ray corresponds to a solid angle about the ray, and is the same for each ray except for the two polar directions.

What remains to be discussed is the method for evaluating the emissivity $\varepsilon_{i+1/2}$ and absorption $\sigma_{a,i+1/2}$ for each segment Δs in eqn.(14). This is the heart of the above ray trace scheme and so an efficient but approximate method was developed. In Lagrangian codes, the emissivity and absorption coefficients are taken to be constant within each cell of the distorted mesh. For the first part of the method, a mapping from the distorted mesh in the computational plane to a rectangular mesh is formulated. The dimensions of

the rectangular mesh are arbitrary with Δr the width of each rectangular cell, Δz the height. Let (K,L) denote the distorted mesh and (I,J) the rectangular mesh. Then for an arbitrary cell (I,J) the mapping [K = KMAP(I,J), L = LMAP(I,J)] gives the cell (K,L) within which the center of cell (I,J) lies. This mapping is calculated once for a distorted mesh. Next, the entire computational volume is embedded in a X'-Y'-Z' Cartesian coordinate system with the plane of the computational mesh lying in the Y'-Z' plane. Now for each segment Δs of a ray in eqn.(14) the corresponding direction cosines of this ray can be used to determine the midpoint $r\text{-}s_{i+1/2}\Omega$ = (X',Y',Z') of the segment Δs. The plasma variables at this midpoint are the same as those at the point ($R = \sqrt{(X'^2+Y'^2)}$, Z = Z') in the computational plane. Division of R by Δr and Z by Δz then gives the cell (I,J) within which the point (R,Z) lies, and finally by the above mapping, a computational cell (K,L). Once this computational cell has been determined the emissivity and absorption coefficients for the segment Δs are known. It is obvious that although the point (R,Z) lies in cell (I,J), and the center of cell (I,J) lies in cell (K,L), it is not necessarily true that the point (R,Z) lies in cell (K,L). Hence, improper values for the coefficients could be used. For gentle gradients in the coefficients this problem would not be severe, while for steep gradients an increase in the dimensions of the rectangular mesh would minimize the errors. For the present problem with steep gradients we used a 40x40 rectangular mesh. Clearly the cost of even doubling the mesh is minimal in storage and computation time.

The results of the ray tracing scheme for the radiation energy density (ERAD) and normalized radiation flux in the z-direction (FZ/c*ERAD) are shown in Figs.5a and 5b, respectively. The parameters NCOSTH and NPHI for the set of rays are shown within the square brackets of Fig.5a. The radiation flux is calculated from the defining eqn.(8).

D. Discussion.

Let us first compare the results for the radiation energy density in Figs.3a, 4a, and 5a. The quantity in parentheses at the top of each contour plot is the total radiation energy within the computational volume. The diffusion result is high by ~19% and the ray trace result is low by ~7%, compared to the closed form results. This tendency is reflected in the contour plots where the diffusive solution has too high an energy density near the axis and in the outer regions. A study of the point by point errors shows that the fractional error of the diffusive solution increases as one moves away from the source surface to over +80% near R = 1 cm, while the ray trace errors are somewhat random and have typical extremes of ±20%. The relative smoothness of the diffusion result compared to the ray trace result is due to the fact that this simple test problem is well suited for a diffusion approach: the entire source is concentrated in a region and the energy density naturally decreases away from this region.

A comparison of the normalized radiation flux in the z-direction from Figs. 3b, 4b, and 5b clearly shows the inadequacy of a diffusion scheme using a flux-limiter to estimate the radiation flux.

To show the effect of increasing the number of rays, this problem was redone using the ray trace approach with ~10 times more rays, but with the same size rectangular (I,J) mesh and number of segment divisions (NSRAY) for each ray as above. The result for the radiation energy density is given in Fig.6, which is nearly identical to the closed form solution.

E. Further Problems and Solutions.

To further compare the diffusion and ray trace schemes we consider several more intricate distributions for the absorption and emission coefficients.

For the next test problem consider the same configuration as the above problem but add a purely absorbing torus with $\sigma_a = 20.0\ cm^{-1}$ extending from 0.3 cm to 0.4 cm in the radial direction and from 0.4 cm to 0.6 cm in the z-direction. This feature should create a shadow immediately behind the absorbing torus away from the source core. We employ a rectangular mesh in the computational plane for this and the following problem to accomadate the configurations. The solutions from the diffusive and ray trace schemes are shown in Figs.7a and 7b, respectively. Again the diffusion scheme gives a higher total radiation energy in the computational volume than the ray trace scheme. More significant is the unphysical character of the energy density contour levels for the diffusive solution. In front of the absorbing torus, i.e., toward the source region, one sees in Fig.7a that the 40 and 35 $ergs/cm^3 \cdot Hz$ contours are attracted toward the torus. Behind the torus, the expected shadow is not seen; instead one finds a radiation energy density between 5 and 10 $ergs/cm^3 \cdot Hz$. Note for the ray trace solution that the contour levels have a reasonable structure in front of the torus, and the shadow is well defined. The erroneous features of the diffusive solution are due to the approximation of the radiative transfer equation as a diffusion equation. In a diffusion process local minimums tend to fill in. For this problem, ∇E at the edges of the shadow are not in the direction of the radiation flux. Hence any flux-limiting diffusion scheme will have difficulties handling shadows.

For the final problem let an emissivity of 100 ergs/cm^{-2}·sec·Hz be confined to two square tori centered about the symmetry axis, and each extending from 0.2 to 0.4 cm in radius. In the *z*-direction, the lower one extends from 0.2 cm to 0.4 cm, and the upper one from 0.6 cm to 0.8 cm. Outside of these tori the emissivity is zero. Let the absorption coefficient be σ_a = 1 cm^{-1} throughout the volume, including the emitting tori. This configuration could model two hot spots formed during a collapsing Z-pinch. The radiation energy density from the numerical results of the diffusion and ray trace schemes are shown in Figs.8a and 8b, respectively. As is typical, the diffusion result gives ~50% more radiation energy integrated throughout the whole volume than does the ray trace solution. This is manifested by the higher values for the contours in the outer regions, between the tori, and near the symmetry axis. In terms of a local heating rate for a plasma, given by $c \cdot \sigma_a \cdot E - 4\pi \cdot \varepsilon$, the results indicate that the heating rate based on the diffusion scheme is greater than a factor of two compared to the ray trace scheme in these regions. The results for the ray trace scheme remain basically unchanged using four times the number of rays of Fig.8b.

III. CONCLUSIONS.

We have presented a comparison of two different numerical methods for solving the radiative transfer equation in axisymmetric geometries. The solutions for these two schemes were compared with a closed form solution of a simple, steady state test problem, and were further compared against each other for several additional problems of more complex spatial configurations.

There are several potential advantages of the diffusive approach over the ray trace approach. First, since these schemes are intended for use in 2-D, cylindrical, radiation-hydrodynamic codes, the time step plays a role. For the implicit diffusive approach, the time step of eqn.(13) is simply that of the hydrodynamic part of the code. The present ray trace scheme, however, does not take account of the photon travel time. For laboratory plasma experiments as mentioned in the Introduction, the spatial size is small enough that a streaming photon will leave the region of interest. Under these conditions the radiation energy density is small compared to the plasma thermal energy density, except possibly in optically thick regions. The time of flight problem is potentially more serious in many astrophysical problems due to the large length scales. In such cases a diffusion approach could follow a travelling radiation front.

Second, if scattering is an important process, the diffusion eqns.(7) and (11) can readily account for it. This is clearly not so for the ray trace scheme where an iteration on the radiation energy density would need to be employed.

The diffusive approach can also accomodate general boundary conditions, such as periodic in one direction or reflective at a boundary. The ray trace scheme is limited in that the incident intensity upon a boundary of the computational volume must be known a priori. This limitation is negated if

the experimental region of interest can be enclosed in the computational volume without reflective boundaries.

Fourth, a diffusive approach provides smoother solutions than a ray trace one by its very nature: local extrema are reduced and local minima are filled in.

However, there are major advantages of the ray trace approach over the diffusive one. First, as the test problems show, the present diffusive scheme can overestimate the radiation energy density, particularly in optically thin, streaming regions. This reflects the fact that in such regions the radiation diffusion velocity of eqn.(12) is always small compared to the speed of light, except in regions of steep radiation energy gradients. Possible corrections for this problem have been referenced in section II.B., but they all have fundamental problems in purely absorbing regions. The consequence of this problem for radiation-hydrodynamic codes would be an overestimate of the plasma heating rate due to absorption. Furthermore, shadows caused by absorbing spots are not at all treated correctly, as evidenced by comparing Figs.7a and 7b.

Second, unlike a diffusive scheme, a general ray trace scheme as described in section II.C. can easily be adjusted to check for accuracy by increasing the number of rays. On the other hand, the number of rays can be reduced to speed computation. There is no such adaptibility in a diffusive approach. We note that the present code can be reduced to the simpler ray trace scheme of Colombant and Winsor[4,5] by limiting the number of rays in the azimuthal direction to two (NPHI=2).

Finally, the present diffusive scheme is roughly 5 to 10 times faster than the ray trace scheme for ~65 rays and a single frequency over a 11x10 computational mesh. However, if a multi-frequency calculation is required for the radiation-hydrodynamics code, then the ray trace scheme would be

faster for more than ~10 frequencies. This is due to the fact that in the ray trace code little extra computation is needed for more than one frequency: in integrating the transfer equation along a ray, a simple vectorizable "do loop" over the frequencies at each segment Δs suffices. On the other hand, for any diffusion approach the diffusion equation must be solved over the whole mesh for each frequency.

ACKNOWLEDGEMENTS

It is a pleasure to thank Drs. John Apruzese, Jack Davis and Robert Clark of the Plasma Radiation Branch for several fruitful discussions and suggestions on this research project. This work was supported by the Defense Nuclear Agency.

REFERENCES

1. D. Duston, R. W. Clark, J. Davis, and J. P. Apruzese, Phys. Rev. A., 27, 1441, "Radiation Energetics of a Laser-Produced Plasma," (1983).

2. J. L. Giuliani, Jr. and M. Mulbrandon, NRL Memo Report #5762, "Numerical Simulation of the Laser-Target Interaction and Blast Wave Formation in the DNA/NRL Laser Experiment," (1986).

3. J. Davis, C. Agritellis, and D. Duston, NRL Memo Report, #5615, "SIMPLODE: An Imploding Gas Puff Plasma Model I. Neon," (1985).

4. D. G. Colombant and N. K. Winsor, NRL Memo Report #2946, "An Accurate Economical Numerical Radiation Transport Algorithm," (1974).

5. D. G. Colombant and N. K. Winsor, NRL Memo Report #2984, "Radiation Transport in Axisymmetric Geometries," (1975).

6. D. G. Colombant, K. G. Whitney, D. A. Tidman, N. K. Winsor and J. Davis, Phys. Fluids, 18, 1687, "Laser Target Model," (1975).

7. G. C. Pomraning, Radiation Hydrodynamics, (Oxford: Pergamon Press), (1973).

8. J. R. Buchler, J. Quant. Spectrosc. Radiat. Transfer, 30, 395, "Radiation Transfer in the Fluid Frame," (1983).

9. D. Mihalas, L. H. Auer, and B. R. Mihalas, Astrophys. J., 220, 1001, "Two-Dimensional Radiative Transfer I. Planar Geometry," (1978).

10. D. Mihalas and R. I. Klein, J. Comp. Phys., 46, 97, "On the Solution of the Time-Dependent Inertial Frame Equation of Radiative Transfer in Moving Media to O(v/c)," (1982).

11. C. D. Levermore and G. C. Pomraning, Astrophys. J., 248, 321, "A Flux-Limited Diffusion Theory," (1981).

12. G. C. Pomraning, J. Quant. Spectrosc. Radiat. Transfer, 26, 385, "Maximum Entropy Eddington Factors and Flux-Limited Diffusion Theory," (1981).

13. G. C. Pomraning, J. Quant. Spectrosc. Radiat. Transfer, 27, 517, "Flux Limiters and Eddington Factors," (1982).

14. G. C. Pomraning, J. Quant. Spectrosc. Radiat. Transfer, 29, 223, "On the $\nabla \cdot \mathbf{F}$ Variable Eddington Factor-Flux Limited Diffusion Description," (1983).

15. C. D. Levermore, J. Quant. Spectrosc. Radiat. Transfer, 31, 149, "Relating Eddington Factors to Flux Limiters," (1984).

16. H. D. Shay, Lawrence Livermore Laboratory Report UCID-16297, "LASNEX Simulation of X-Ray Generation," (1973).

17. D.S. Kershaw, J. Comp. Phys., 39, 375, "Differencing of the Diffusion Equation in Lagrangian Hydrodynamic Codes," (1981)

18. G. J. Pert, J. Comp. Phys., 42, 20, "Physical Constraints in Numerical Calculations of Diffusion," (1981).

19. K. Hain, NRL Memo Report #4264, "A Non-Recursive Incomplete Cholesky Decomposition Method for the Solution of Linear Equations with a Sparse Matrix," (1980).

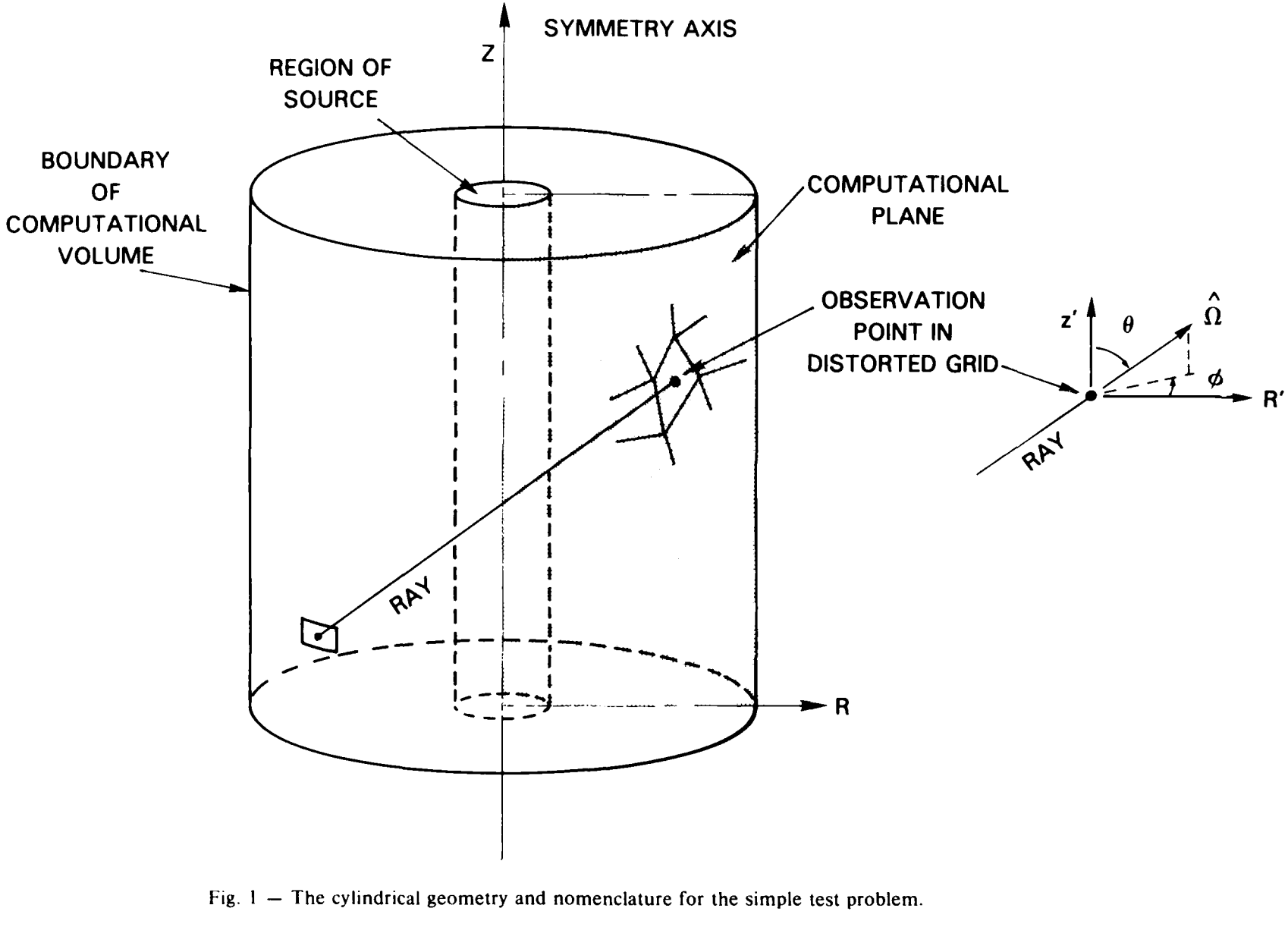

Fig. 1 — The cylindrical geometry and nomenclature for the simple test problem.

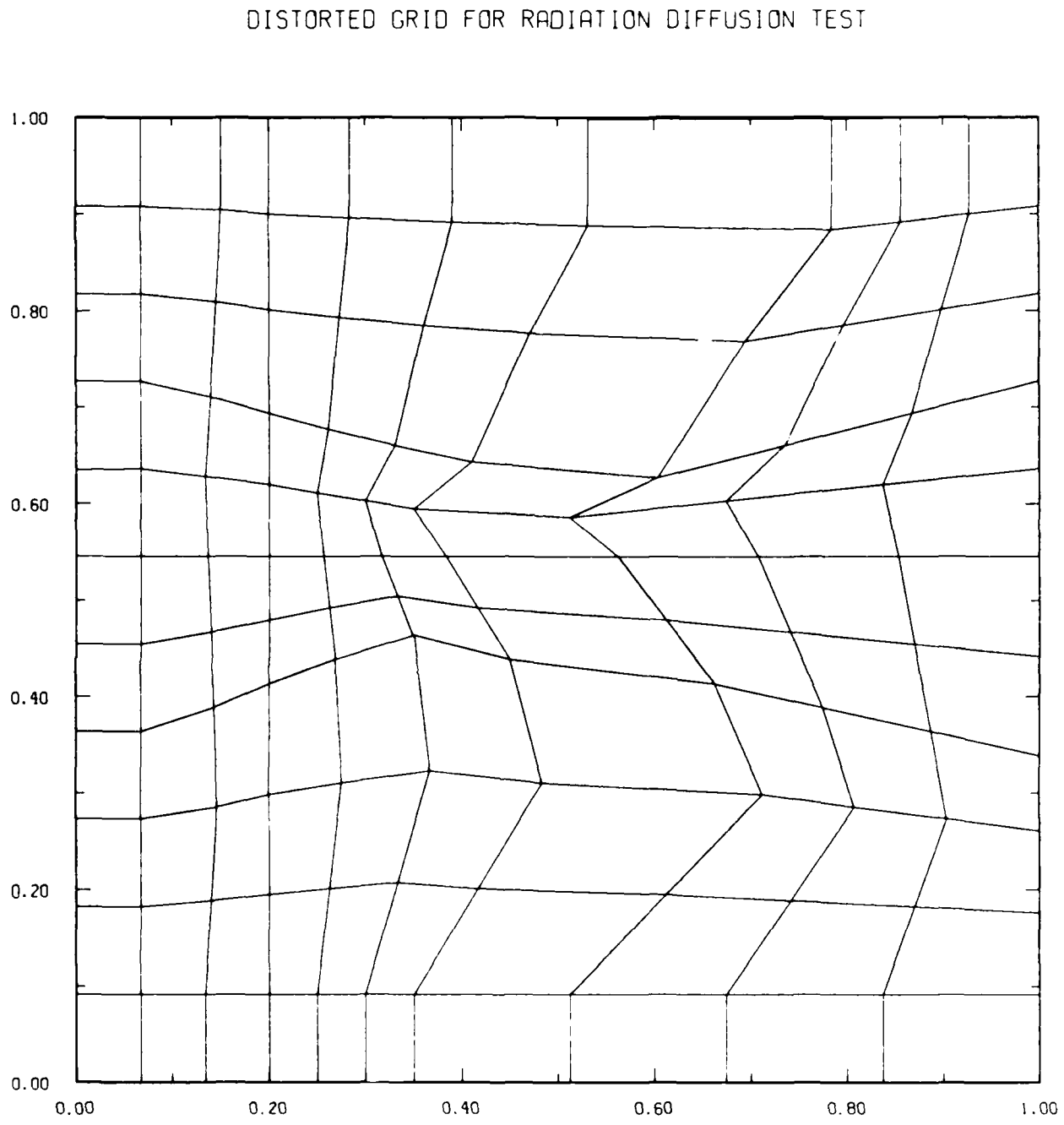

Fig. 2 — The distorted mesh in the computational plane for the simple test problem.

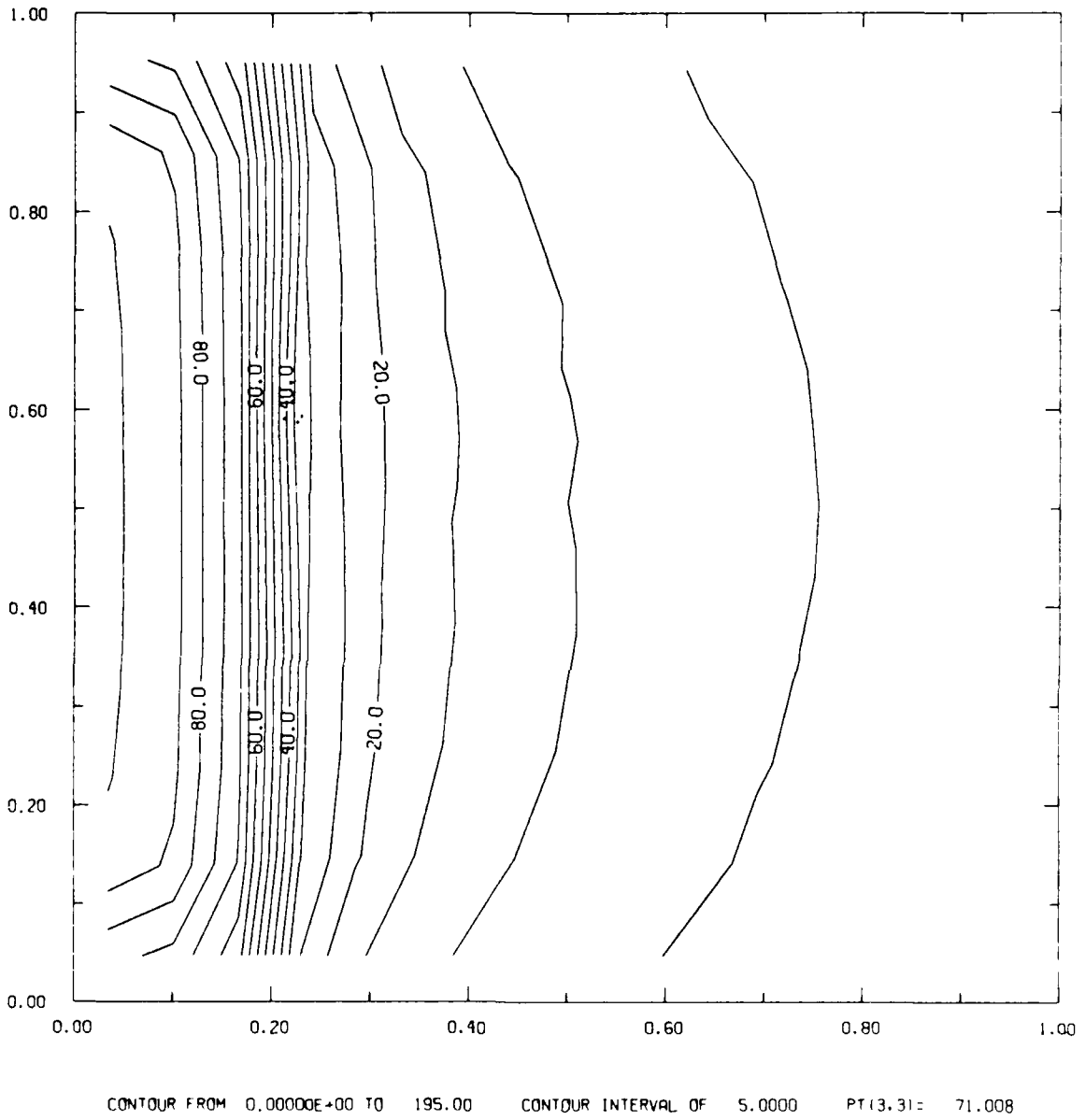

Fig. 3 — The closed form solutions to the simple test problem of a finite height emitting core; (a) the radiation energy density in ergs/cm^3 · Hz, (b) the non-dimensional, normalized radiation flux in the z-direction.

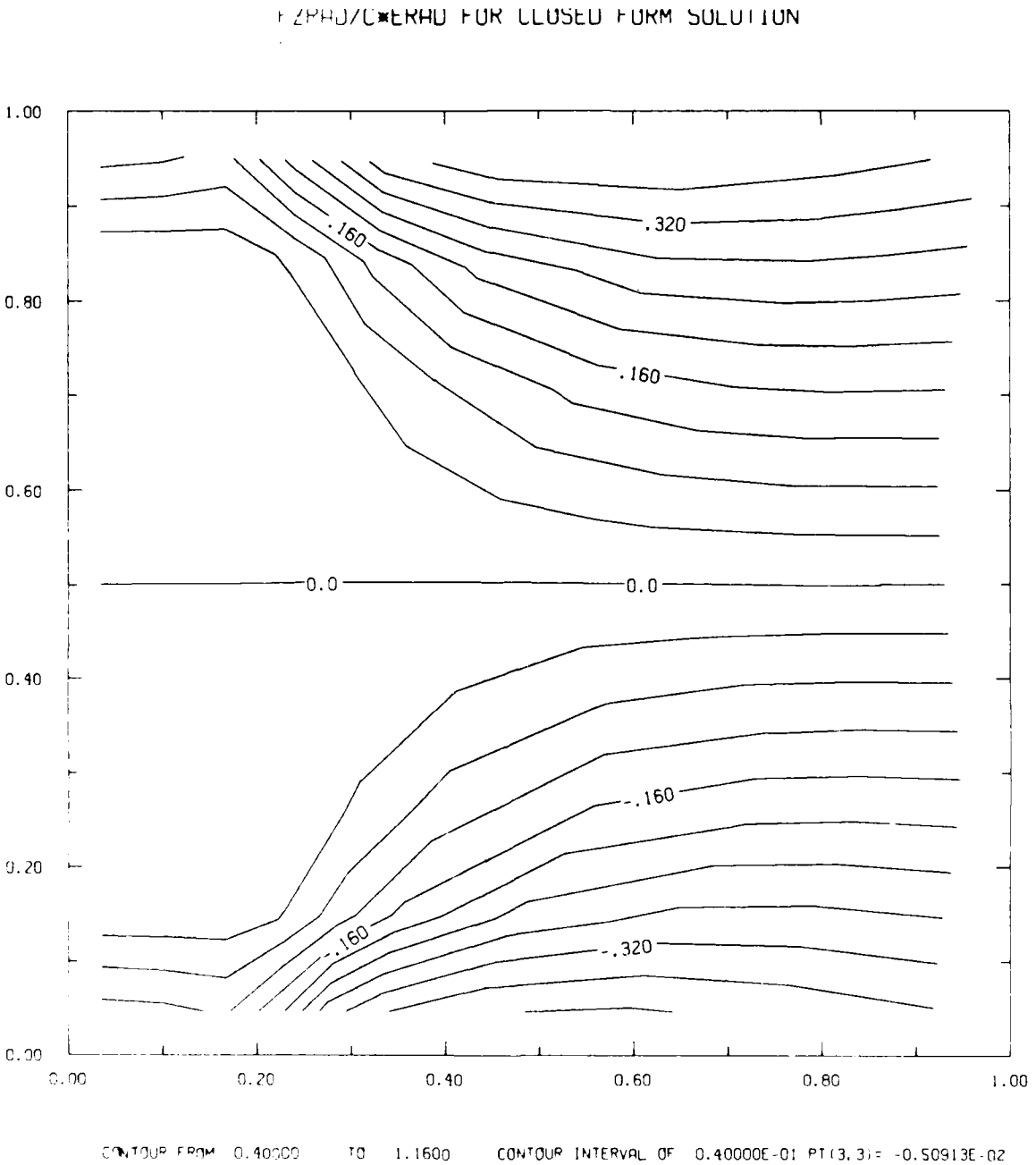

Fig. 3 (Cont'd) — The closed form solutions to the simple test problem of a finite height emitting core; (a) the radiation energy density in ergs/cm^3 · Hz, (b) the non-dimensional, normalized radiation flux in the z-direction.

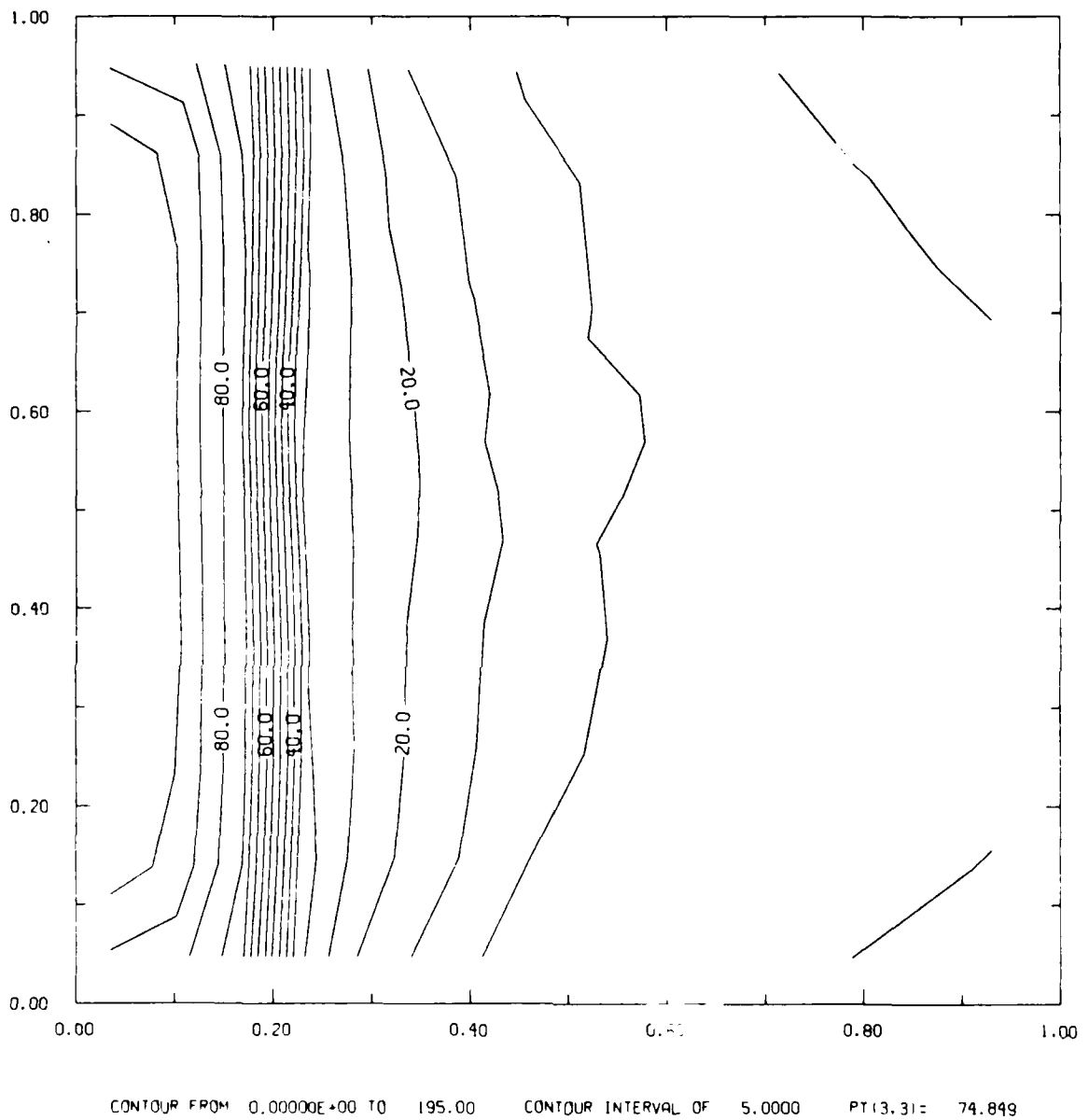

Fig. 4 — The diffusive scheme solutions to the simple test problem after twenty steps; (a) the radiation energy density in ergs/cm^3 · Hz, (b) the non-dimensional, normalized radiation flux in the z-direction.

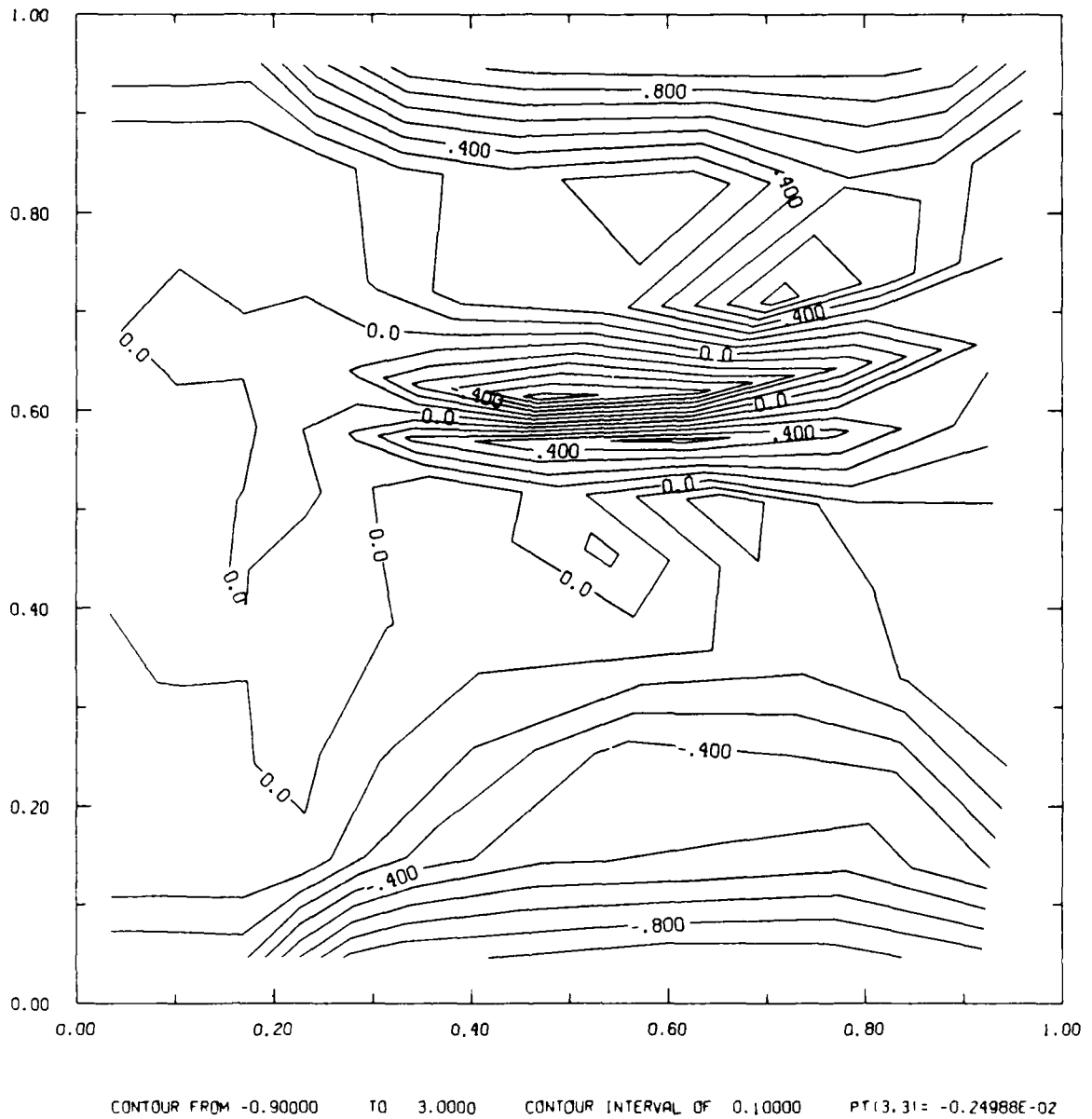

Fig. 4 (Cont'd) — The diffusive scheme solutions to the simple test problem after twenty steps; (a) the radiation energy density in ergs/cm^3 · Hz, (b) the non-dimensional, normalized radiation flux in the z-direction.

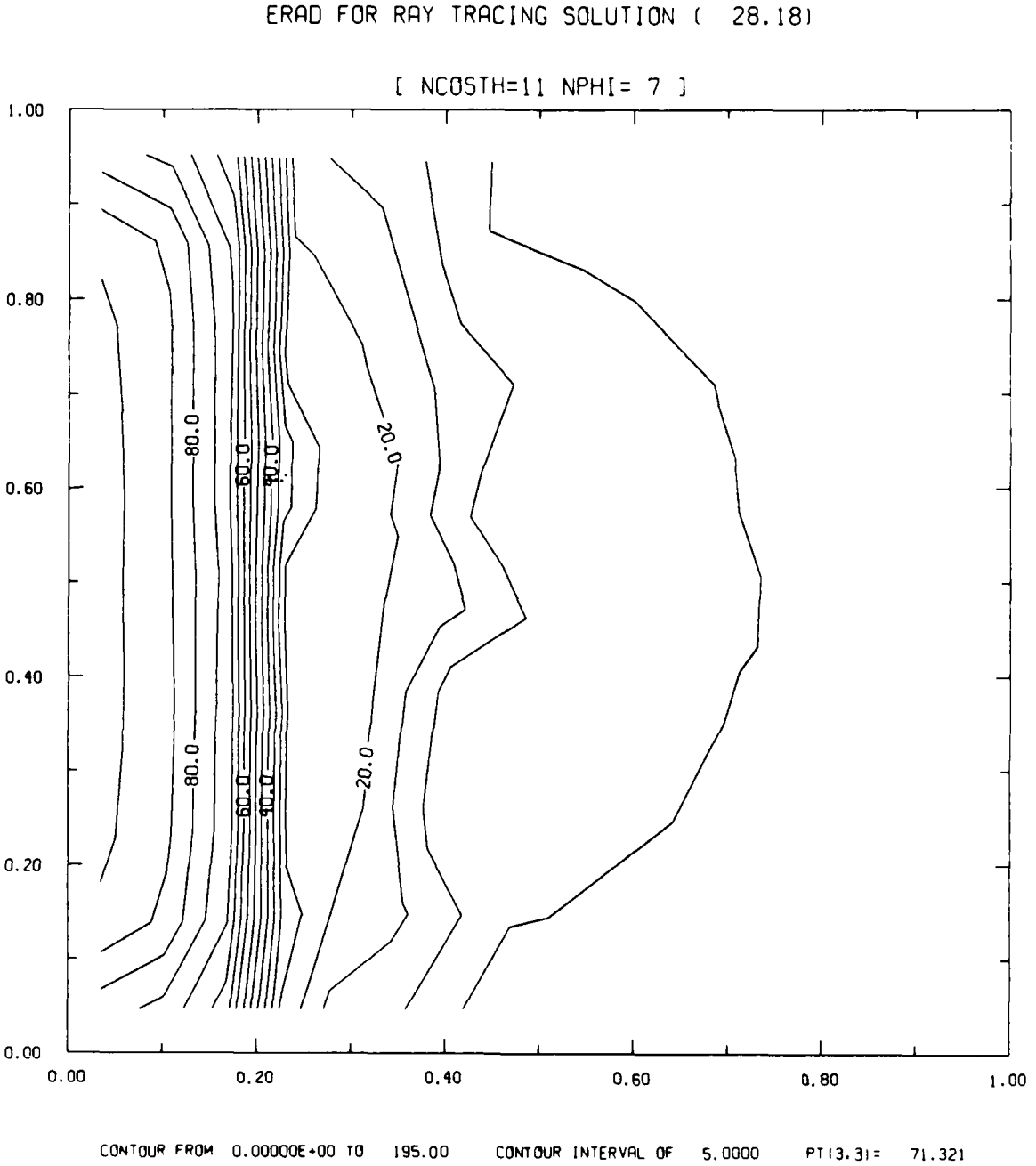

Fig. 5 — The ray trace solutions to the simple test problem; (a) the radiation energy density in ergs/cm^3 · Hz, (b) the non-dimensional, normalized radiation flux in the z-direction.

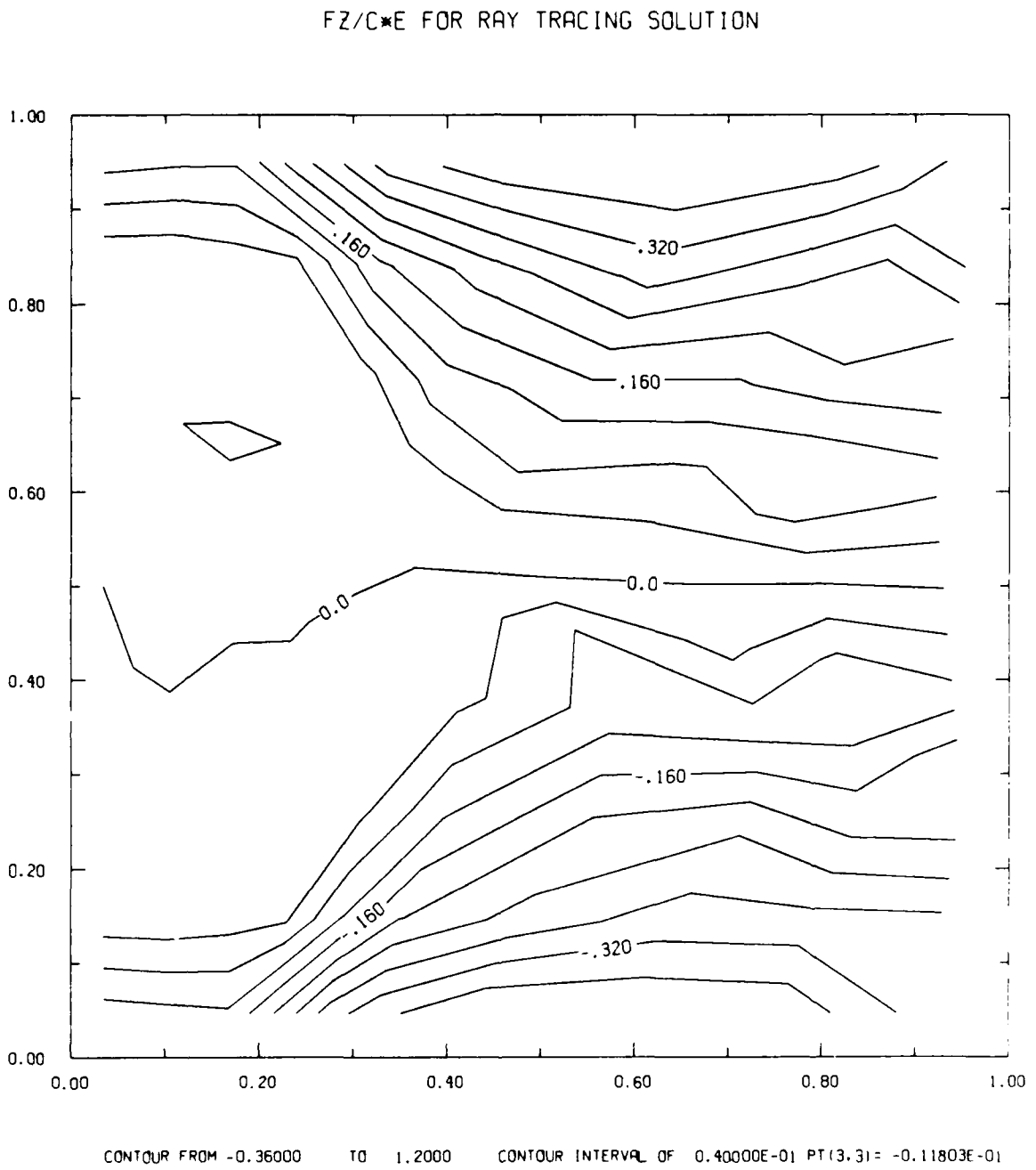

Fig. 5 (Cont'd) — The ray trace solutions to the simple test problem; (a) the radiation energy density in ergs/cm^3 · Hz, (b) the non-dimensional, normalized radiation flux in the z-direction.

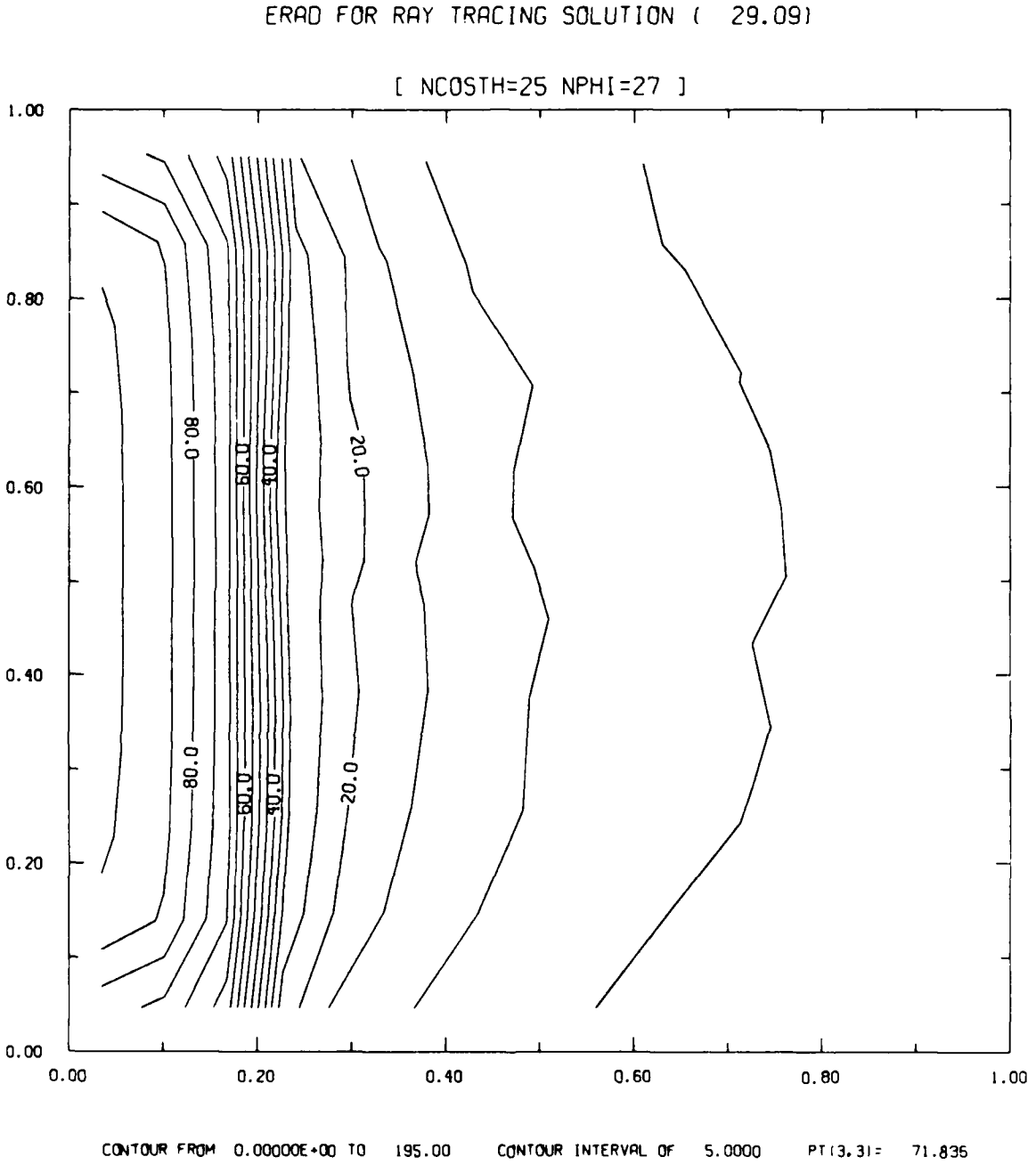

Fig. 6 — The ray trace solution of the radiation energy density for the simple test problem using ~10 times more rays than in Fig. 5a.

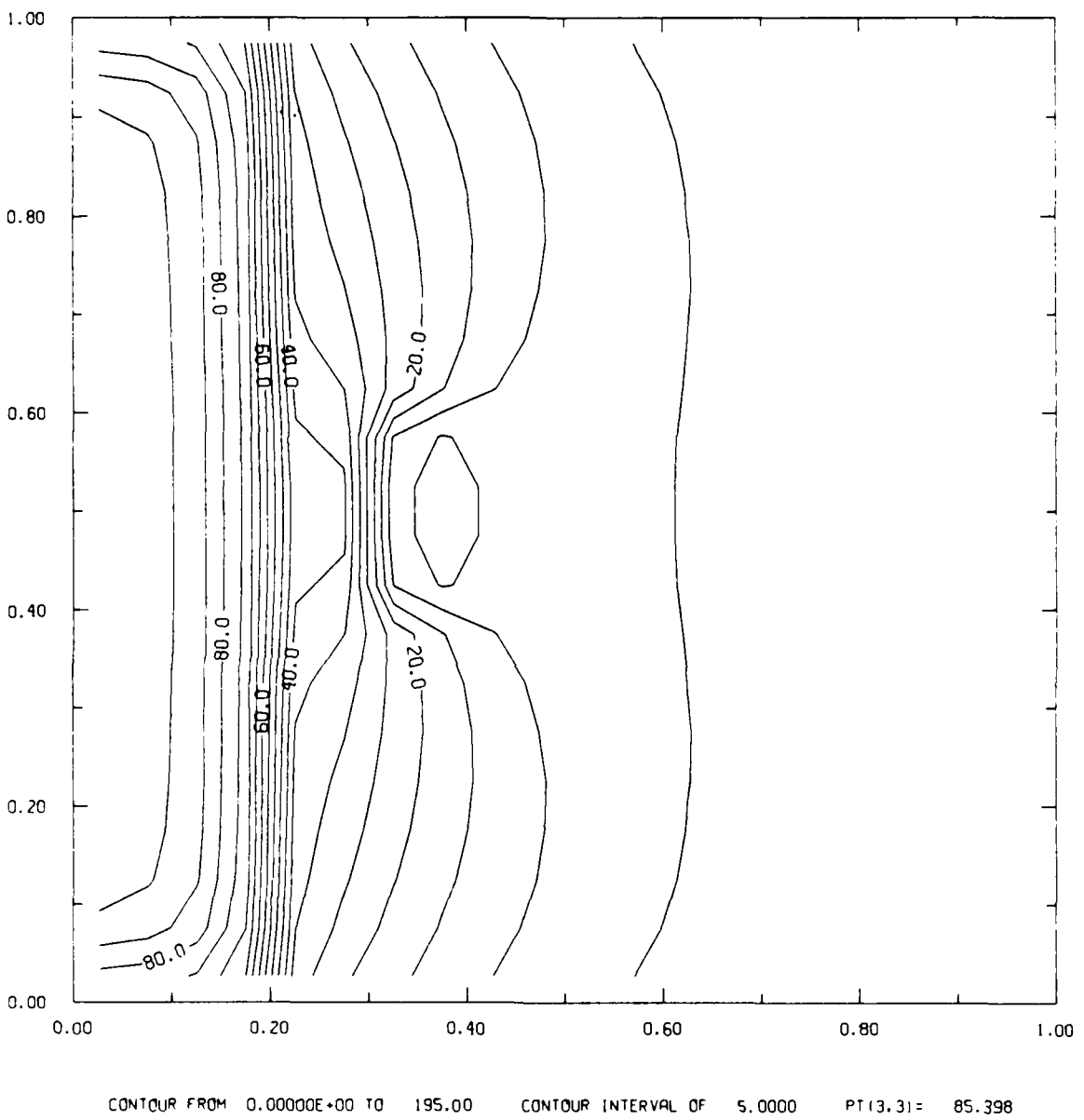

Fig. 7 — The solutions for the radiation energy density of the second test problem with a purely absorbing torus in front of the emitting core; (a) the diffusive solution, (b) the ray trace solution.

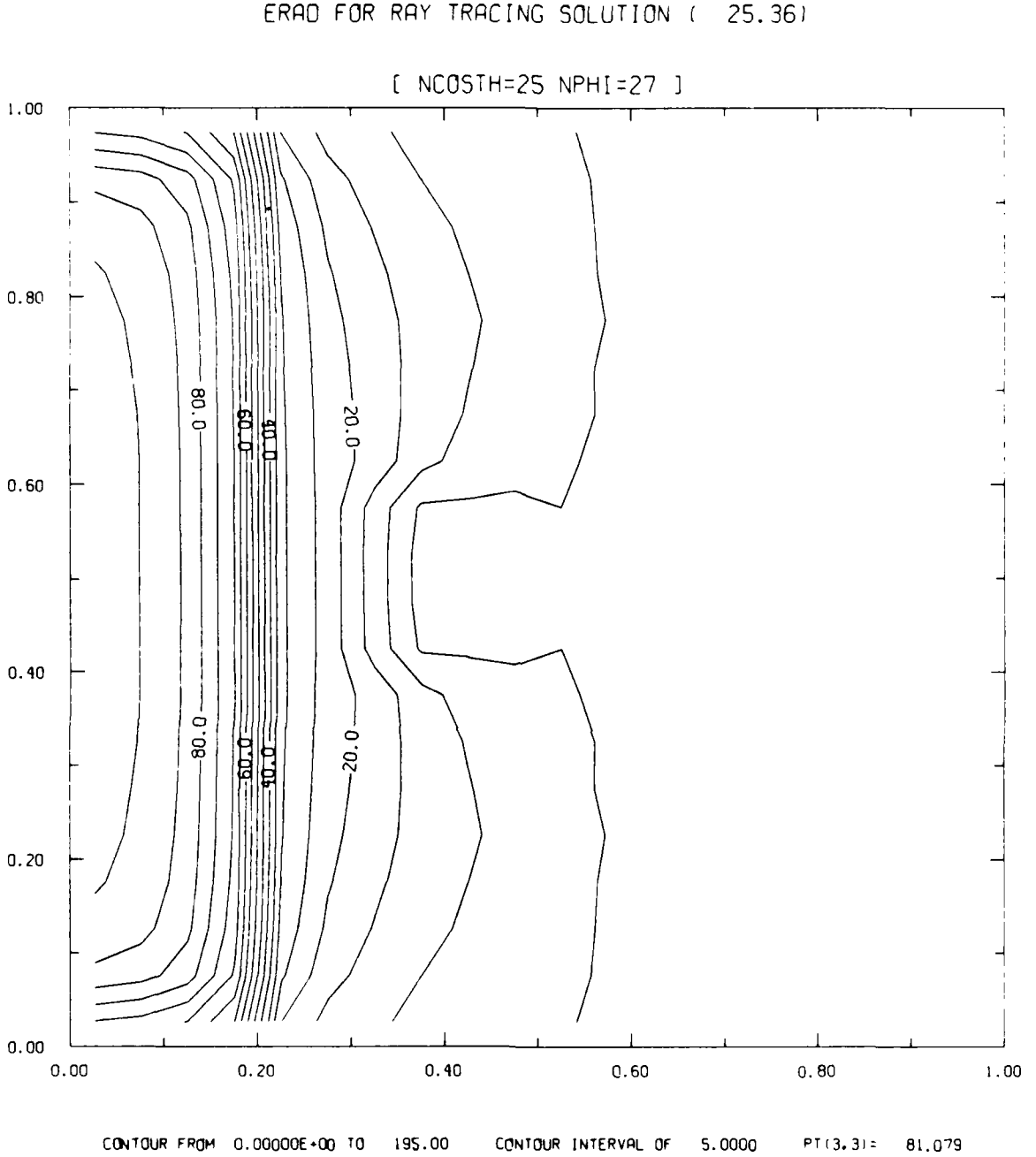

Fig. 7 (Cont'd) — The solutions for the radiation energy density of the second test problem with a purely absorbing torus in front of the emitting core; (a) the diffusive solution, (b) the ray trace solution.

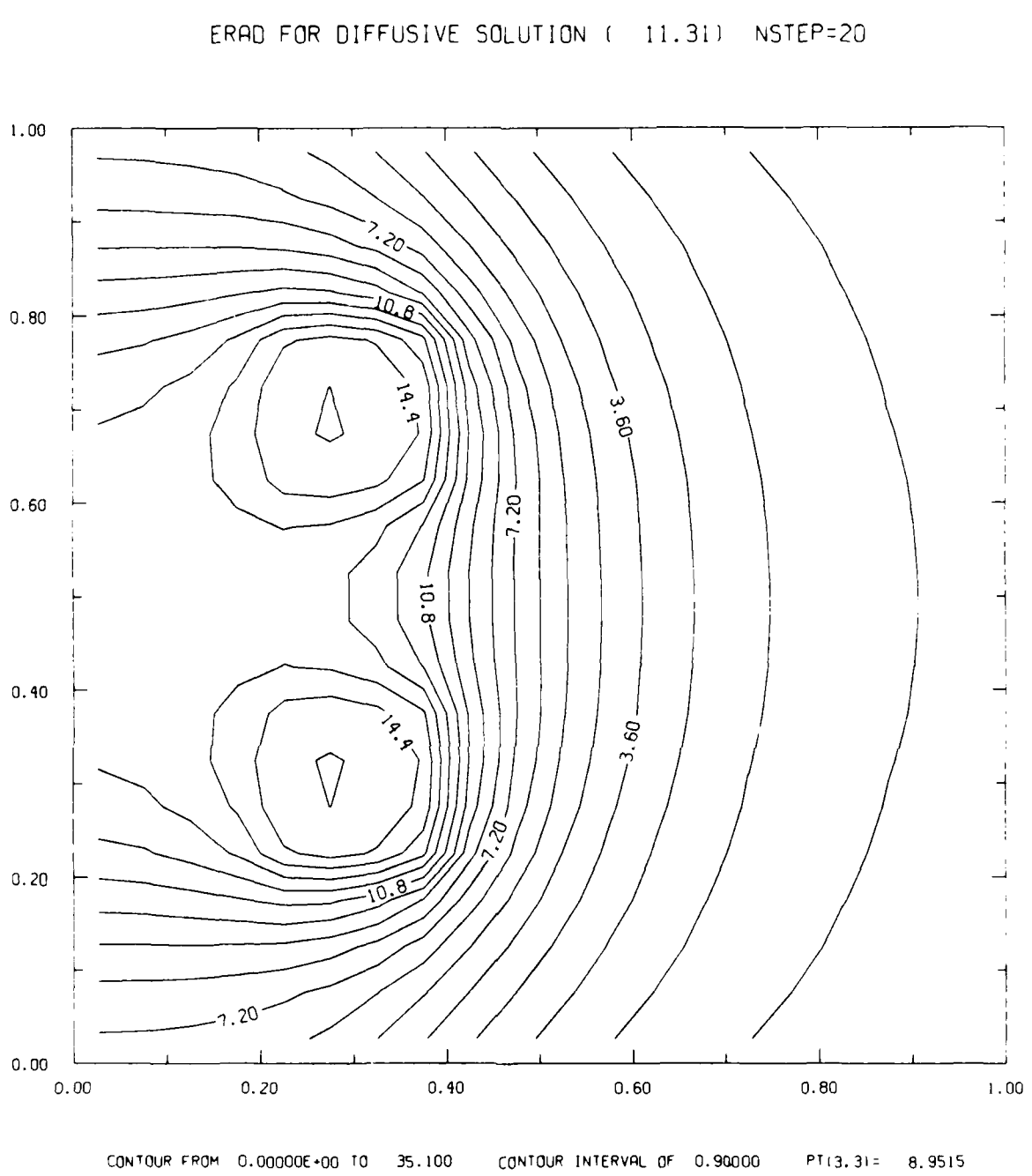

Fig. 8 — The solutions for the radiation energy density of the third test problem with two emitting tori; (a) the diffusive solution, (b) the ray trace solution.

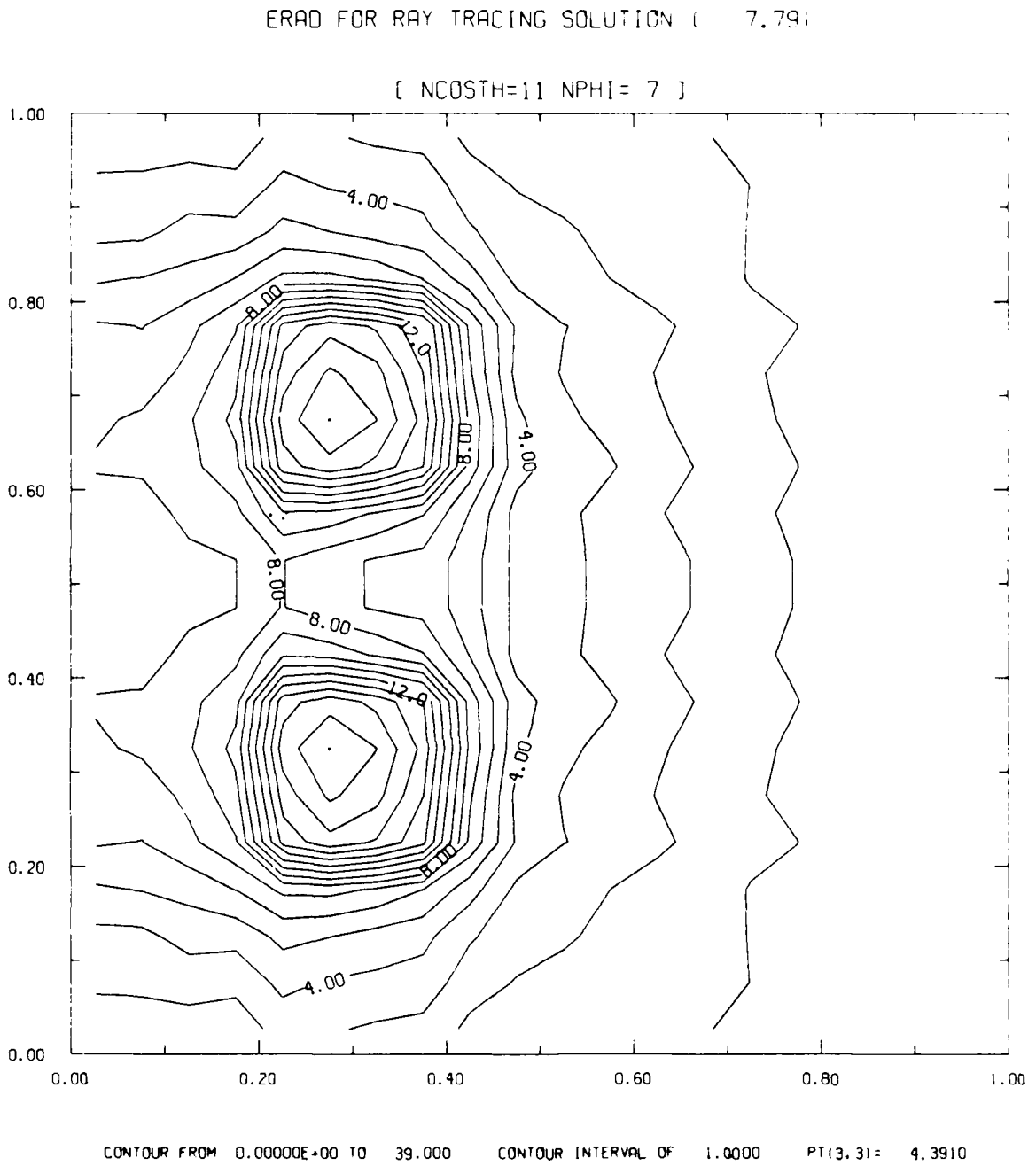

Fig. 8 (Cont'd) — The solution for the radiation energy density of the third test problem with two emitting tori; (a) the diffusive solution, (b) the ray trace solution.

DISTRIBUTION LIST

Assistant to the Secretary of Defense Atomic Energy Washington, D.C. 20301 ATTN: Executive Assistant	1 Copy
Director Defense Intelligence Agency Washington, D.C. 20301 ATTN: DT-1B R. Rubenstein	1 Copy
Director Defense Nuclear Agency Washington, D.C. 20305	
ATTN: DDST	1 copy
ATTN: TITL	4 copies
ATTN: RAEV	1 copy
ATTN: STVI	1 copy
Commander Field Command Defense Nuclear Agency Kirtland AFB, New Mexico 87115 ATTN: FCPR	1 Copy
Chief Field Command Livermore Division Department of Defense P.O. Box 808 Livermore, CA 94550 ATTN: FCPRL	1 Copy
Director Joint Strat TGT Planning Staff Offutt AFB Omaha, Nebraska 68113 ATTN: JLKS	1 Copy
Undersecretary of Defense for RSCH and ENGRG Department of Defense Washington, D.C. 20301 ATTN: Strategic and Space Systems (OS)	1 Copy
Deputy Chief of Staff for RSCH DEV and ACQ Department of the Army Washington, D.C. 20301 ATTN: DAMA-CSS-N	1 Copy

Commander — 1 copy each
Harry Diamond Laboratories
Department of the Army
2800 Powder Mill Road
Adelphi, MD 20783
ATTN: DELHD-N-NP
ATTN: DELHD-R J. Rosado
ATTN: DELHD-TA-L (Tech. Lib.)

U.S. Army Missile Command
Redstone Scientific Information Center — 3 Copies
Attn: DRSMI-RPRD (Documents)
Redstone Arsenal, Alabama 35809

Commander — 1 copy
U.S. Army Missile Command
Redstone Arsenal, Alabama 35898
ATTN: DRCPM-PE-EA

Commander
U.S. Army Nuclear and Chemical Agency
7500 Backlick Road — 1 copy
Building 2073
Springfield, VA 22150
ATTN: Library

Commander — 1 Copy
Naval Intelligence Support Center
4301 Suitland Road, Bldg. 5
Washington, D.C. 20390
ATTN: NISC-45

Commander — 1 Copy
Naval Weapons Center
China Lake, California 93555
ATTN: Code 233 (Tech. Lib.)

Officer in Charge — 1 Copy each
White Oak Laboratory
Naval Surface Weapons Center
Silver Spring, Md. 20910
ATTN: Code R40
ATTN: Code F31

Air Force Weapons Laboratory — 1 Copy each
Kirtland AFB, New Mexico 87117
ATTN: SUL
ATTN: CA
ATTN: APL
ATTN: Lt. Col Generosa

Deputy Chief of Staff — 1 Copy
Research, Development and Accounting
Department of the Air Force
Washington, D. C. 20330
ATTN: AFRDQSM

Commander — 1 Copy
U.S. Army Test and Evaluation Command
Aberdeen Proving Ground, MD 21005
ATTN: DRSTE-EL

AVCO Research and Systems Group — 1 Copy
201 Lowell Street
Wilminton, MA 01887
ATTN: Library A830

BDM Corporation — 1 Copy
7915 Jones Branch Drive
McLean, Virginia 22101
ATTN: Corporate Library

Berkeley Research Associates — 1 Copy
P.O. Box 983
Berkeley, CA 94701
ATTN: Dr. Joseph Workman

Berkeley Research Associates — 1 Copy each
P.O. Box 852
5532 Hempstead Way
Springfield, VA 22151
ATTN: Dr. Joseph Orens

Boeing Company — 1 Copy
P. O. Box 3707
Seattle, WA 98134
ATTN: Aerospace Library

The Dikewood Corporation — 1 Copy
1613 University Bldv., N.E.
Albuquerque, New Mexico 87110
ATTN: L. Wayne Davis

General Electric Company — 1 Copy
Space Division
Valley Forge Space Center
P. O. Box 8555
Philadelphia, PA 19101
ATTN: J. Peden

General Electric Company - Tempo — 1 Copy
Center for Advanced Studies
816 State Street
P.O. Drawer QQ
Santa Barbara, CA 93102
ATTN: DASIAC

Institute for Defense Analyses — 1 Copy
1801 N. Beauregard St.
Alexandria, VA 22311
ATTN: Classified Library

IRT Corporation — 1 Copy
P.O. Box 81087
San Diego, CA 92138
ATTN: R. Mertz

JAYCOR — 1 Copy
11011 Forreyane Rd.
P.O. Box 85154
San Diego, CA 92138
ATTN: E. Wenaas
F. Felbar

JAYCOR — 1 Copy
205 S. Whiting Street, Suite 500
Alexandria, VA 22304
ATTN: R. Sullivan

KAMAN Sciences Corp. — 1 copy each
P. O. Box 7463
Colorado Springs, CO 80933
ATTN: Library

Lawrence Livermore National Laboratory — 1 copy each
University of California
P.O. Box 808
Livermore, California 94550
Attn: DOC CDN for L-153
Attn: DOC CDN for L-47 L. Wouters
Attn: DOC CDN for Tech. Infor. Dept. Lib.

Lockheed Missiles and Space Co., Inc. — 1 copy each
P. O. Box 504
Sunnyvale, CA 94086
Attn: S. Taimlty
Attn: J.D. Weisner

Lockheed Missiles and Space Co., Inc. — 1 Copy
3251 Hanover Street
Palo Alto, CA 94304
Attn: J. Perez

Maxwell Laboratory, Inc. — 1 Copy each
9244 Balboa Avenue
San Diego, CA 92123
ATTN: A. Kolb
ATTN: M. Montgomery
ATTN: J. Shannon

McDonnell Douglas Corp. — 1 Copy
5301 Bolsa Avenue
Huntington Beach, CA 92647
ATTN: S. Schneider

Mission Research Corp. — 1 Copy each
P. O. Drawer 719
Santa Barbara, CA 93102
ATTN: C. Longmire
ATTN: W. Hart

Mission Research Corp.-San Diego — 1 Copy
5434 Ruffin Rd.
San Diego, California 92123
ATTN: Victor J. Van Lint

Northrop Corporation — 1 Copy
Northrop Research and Technology Center
1 Research Park
Palos Verdes Peninsula, CA 90274
ATTN: Library

Physics International Company — 1 Copy each
2700 Merced Street
San Leandro, CA 94577
ATTN: M. Krishnan
ATTN: C. Gilman
ATTN: S. Wong

R and D Associates — 1 Copy each
P.O. Box 9695
Marina del Rey, CA 90291
ATTN: W. Graham, Jr.
ATTN: P. Haas

Sandia National Laboratories — 1 copy each
P. O. Box 5800
Albuquerque, New Mexico 87115
ATTN: Doc Con For 3141
ATTN: D. McDaniel
ATTN: P. VanDevender
ATTN: K. Matzen, Code 4247

Science Applications, Inc. — 1 copy
P. O. Box 2351
La Jolla, CA 92038
ATTN: R. Poyster

Spectra Technol, Inc., — 1 copy
Attn: Alan Hoffman
2755 Northup Way
Bellevue, Washington 98004

Spire Corporation — 1 copy
P. O. Box D
Bedford, MA 01730
ATTN: R. Little

SRI International — 1 copy
333 Ravenswood Avenue
Menlo Park, CA 94025
ATTN: S. Dairiki

S-CUBED — 1 copy
P. O. Box 1620
La Jolla, CA 92038
ATTN: A. Wilson

Director
Strategic Defense Initiative Organization — 1 copy each
1717 H Street
Pentagon 20301-7100
ATTN: DE Lt. Col Richard Gullickson/DEO
IST Dr. Dwight Duston
ATTN: IST Dr. J. Ionson

Texas Tech University — 1 copy
P.O. Box 5404
North College Station
Lubbock, TX 79417
ATTN: T. Simpson

TRW Defense and Space Systems Group — 1 Copy
One Space Park
Redondo Beach, CA 90278
ATTN: Technical Information Center

University of Buffalo
Attn: Professor W. J. Sarjeant — 1 Copy
Dept. of Electrical Engineering
High Voltage and Power
312 Bonner Hall
Buffalo, New York 14260

Naval Research Laboratory
Plasma Radiation Branch
Washington, D.C. 20375
Code 4720 - 50 Copies
Code 4700 - 26 Copies
Code 2628 - 22 Copies

END

12-86

DTIC